Journal of the European Ceramic Society 37 (2017) 975–983

Contents lists available at www.sciencedirect.com

Journal of the European Ceramic Society

journal homepage: www.elsevier.com/locate/jeurceramsoc

Investigations of domain switching and lattice strains in (Na,K)NbO_3-based lead-free ceramics across orthorhombic-tetragonal phase boundary

Jian Fu [a], Ruzhong Zuo [a,*], Yudong Xu [a], Jing-Feng Li [b], Min Shi [a]

[a] Institute of Electro Ceramics & Devices, School of Materials Science and Engineering, Hefei University of Technology, Hefei 230009, PR China
[b] State Key Laboratory of New Ceramics and Fine Processing, School of Materials Science and Engineering, Tsinghua University, Beijing 100084, PR China

ARTICLE INFO

Article history:
Received 9 September 2016
Received in revised form 15 October 2016
Accepted 17 October 2016
Available online 19 October 2016

Keywords:
Piezoelectricity
Strain
X-ray diffraction
Domain switching

ABSTRACT

Various strain contributions of $(Na_{0.52}K_{0.48-x})(Nb_{0.92-x}Sb_{0.08})O_3 - xLiTaO_3$ ceramics in the proximity of orthorhombic (O) and tetragonal (T) polymorphic phase boundary (PPB) were quantitatively resolved by means of synchrotron x-ray diffraction together with macroscopic strain measurements. Compared with O-rich compositions with a governing mechanism of intrinsic lattice strains, T-rich compositions exhibited a dominant strain mechanism from reversible domain switching. Quantitative analysis of diffraction data suggested that extrinsic strain contributions should depend on not only the lattice distortion δ, but also the poling texture Δf, phase content (for PPB compositions) and domain types. Smaller lattice distortion and higher poling texture tended to enhance the number of irreversible domain switching in O-rich compositions, thus leading to larger fraction of intrinsic lattice strain contribution. The calculated results demonstrated that the product of two parameters Δf and δ would give a reliable estimation of domain-switching strains for T-phase compositions but an overestimation for O-phase compositions.

1. Introduction

Actuators that transform electrical excitation signal into controlled displacement have been widely used in fuel injectors, ink-jet printers, autofocusing of cameras and so on. Piezoelectric ceramics as one of the most important actuator materials are commonly based on $Pb(Zr,Ti)O_3$ (PZT)-based ceramics close to a ferroelectric rhombohedral (*R*)-tetragonal (T) morphotropic phase boundary (MPB) [1–3]. Recently, because of the health and environmental concerns, much attention has been focused on developing lead-free alternatives with large strains for actuator applications.

(Na,K)NbO_3 (NKN) based piezoelectric system has been considered as one of the most promising lead-free candidates because of their attractive piezoelectric properties and relatively high Curie temperatures. Large piezoelectric coefficients ($d_{33} \sim 250–400$ pC/N) were reported to appear in the vicinity of polymorphic phase boundary (PPB) separating orthorhombic (O) phase from T phase [4–7]. Large piezoelectric strains (~0.12–0.16%) comparable to those of lead-based MPB compositions could be obtained in NKN-based PPB compositions, thus making them also suitable for actuator devices [8–10]. Most of studies in this field have been so far focused on the compositional modification to improve the strain response of NKN-based lead-free materials [11–15]. There has been few systematic investigation of the strain mechanism involved in these lead-free compositions till now, particularly on the relation of strain contributions to changes in structural characteristics. Although a high strain level of ~0.15% was reported in $(Na_{0.52}K_{0.48-x})(Nb_{0.92-x}Sb_{0.08})O_3 - xLiTaO_3$ (NKNS-xLT) ceramics [9], yet strain values showed a strong composition dependence, especially during the period of the O-T phase structural change. The composition dependence of the strain behavior and understanding of physical mechanisms underlying the measured macroscopic strains are therefore issues of major concerns for the design of NKN-based lead-free piezoceramic actuators. Piezoelectric ceramic actuators usually work under a large-signal electric loading, leading to a non-linear electromechanical response because of domain switching, as evidenced by a certain degree of strain hysteresis and non-linearity of S-E unipolar loops. In fact, the strain response of piezoelectric ceramics usually arises from the electromechanical coupling effect [3,16–19], including both intrinsic piezoelectric lattice strains and extrinsic strains from non-180° domain switching. In-situ x-ray diffraction (XRD) was considered as a powerful method for quantifying these two processes for a couple of Pb-

* Corresponding author.
E-mail addresses: piezolab@hfut.edu.cn, rzzuo@hotmail.com (R. Zuo).

http://dx.doi.org/10.1016/j.jeurceramsoc.2016.10.024
0955-2219/

based piezoelectric materials [20–26]. Piezoelectric lattice strain is usually accompanied by a shift of diffraction peak positions due to the expansion (or contraction) of unit cells while non-180° domain switching results in the variation of peak intensities due to the domain reorientation along the electric field direction.

The objective of this work is to analyze various strain contributions from domain switching and piezoelectric effect for a few typical NKNS-xLT lead-free ceramics by means of high-energy synchrotron XRD in combination with the measurement of macroscopic strains. Differences between these materials mainly involve the characteristics of composition-induced changes in crystallographic structure, including lattice distortion, phase structure and content, type of domains and poling texture. The interpretation of the XRD patterns was based on a conventional structural model assuming PPB compositions are composed of O and T phases. No attempts were made to take into account the presence of any intermediate phase.

2. Experimental

NKNS-xLT ceramics (x = 0.01–0.06) were synthesized by a conventional solid-state reaction route as described elsewhere [7]. Sintering was carried out in air in the temperature range of 1100 °C–1120 °C for 3 h at a heating rate of 5 °C and a cooling rate of 10 °C, respectively. The sample densities were evaluated by the Archimedes method. The microstructure was observed by using a scanning electron microscope (SEM, JEOL JSM-6490LV, Tokyo, Japan). The domain structure was analyzed by using a transmission electron microscope (TEM, Phillips CM-20, Hillsboro, OR) operated at 200 kV with a charge coupled device camera. Specimens for TEM studies were prepared from bulk ceramics by mechanically polishing to ~20 μm and then ion-milling on a Gatan Dual Ion Mill unit (Model 600) at 5 kV.

For the measurement of electrical properties, the as-sintered ceramics were ground and polished to a thickness of ~0.5 mm and then were annealed at 500 °C for 4 h at a heating rate of 5 °C and a cooling rate of 5 °C, respectively, to remove mechanical stress. Silver paste was painted on both major surfaces and then fired at 600 °C. Both polarization-electric field (P-E) hysteresis loops and strain-electric field (S-E) curves under unipolar and bipolar electric fields were measured at room temperature using a ferroelectric testing system (Premium II, Radiant Technologies Inc., Albuquerque, NM) connected with a laser interferometric vibrometer (SP-S 120, SIOS Meβtechnik GmbH, Germany).

For ex-situ XRD measurements, the conductive adhesives were screened on two polished surfaces and then dried. These samples were then poled under a dc electric field of 3 kV/mm for 15 min at room temperature. For in-situ XRD measurements, gold electrodes were sputtered onto two major sides of polished samples. Moreover, some of the as-sintered samples were crushed and further milled for the powder XRD measurement. Powder XRD, ex-situ XRD (poled under 3 kV/mm) and in-situ XRD under 0 and 3 kV/mm were taken at room temperature at beamline BL14B1 (λ = 1.2378 Å) at Shanghai Synchrotron Radiation Facility. Measurements were performed by θ-2θ step-scans using a Huber 5021 six-circle diffratometer with a NaI scintillation detector.

3. Results

3.1. Crystallographic variants of NKNS-xLT ceramics

Fig. 1 shows the sketch of the typical crystal structures of ABO_3 perovskite unit cells. A prototypical perovskite structure with a cubic symmetry above the Curie temperature transforms into either a T phase with a spontaneous polarization along $[001]_c$ direction or an O phase with $[101]_c$ spontaneous polar axis upon decreasing temperature. This depends on the LT content x for NKNS-xLT ceramics. Difference in the lattice distortion between O and T phases leads to their different diffraction patterns, as more clearly seen in 200_c and 222_c reflections. On the one hand, 200_c doublet can be observed in both O and T phases, corresponding to $202_o/020_o$ reflections and $002_t/200_t$ reflections, respectively. However, the intensity of the 202_o reflection is roughly twice more than that of the 020_o reflection, while the intensity of the 002_t reflection is almost half of the 200_t reflection. On the other hand, a single reflection corresponding to the 222_t can be observed in T phase, while O phase exhibits an obvious 222_c doublet corresponding to the $22\text{-}2_o$ and 222_o reflections because the symmetry of the O phase subcell is monoclinic.

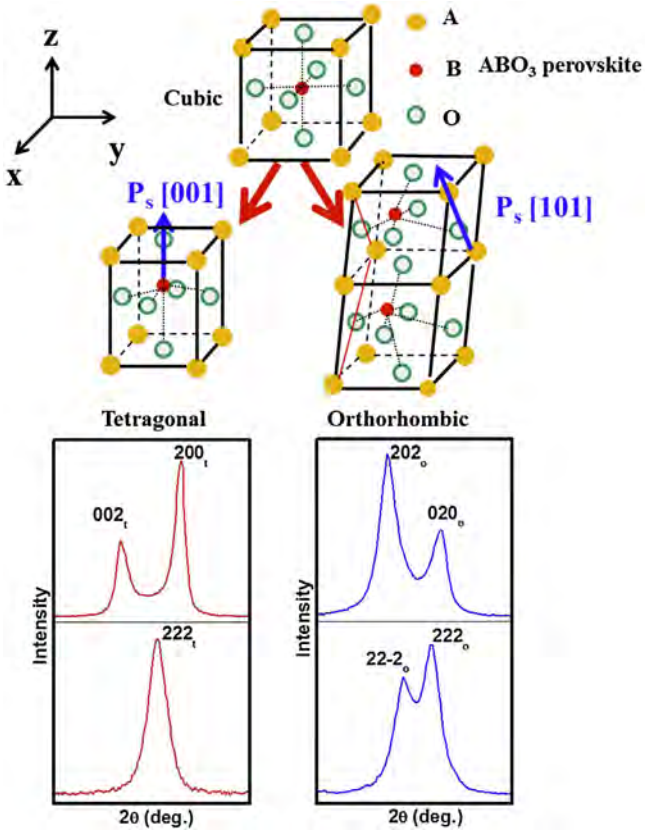

Fig. 1. The sketch of the crystallographic structures of ABO_3 perovskite with corresponding diffraction patterns of 200_c and 222_c reflections for T and O phases.

The magnitude of spontaneous strains in a ferroelectric is usually approximated by its lattice distortion. The lattice distortion of T phase (δ_t) can be determined according to the splitting of 200_c reflections:

$$\delta_t = \frac{c_t}{a_t} - 1 = \frac{d_{002_t}}{d_{200_t}} - 1 \quad (1)$$

By comparison, the determination of the lattice distortion of O phase (δ_o) is more complicated because lattice parameters of O phase strongly depend on the splitting of both 200_c reflections and 222_c reflections [27]. To simplify the calculation, δ_o can be determined by the monoclinic subcell as follows:

$$\delta_o = \frac{c_m}{b_m} - 1 = \frac{c_o/\sqrt{2}}{b_o} - 1 \left(c_o = a_m \cos\frac{\beta}{2} + c_m \cos\frac{\beta}{2} \right) \quad (2)$$

The a_m (c_m) and b_m in a monoclinic perovskite subcell are obtained using the following relations:

$$a_m = c_m = \frac{2d_{002_m}}{sin\beta} \text{ and } b_m = 2d_{020_m} \quad (3)$$

The β angle can be calculated using the equation as follows:

$$\beta = \arccos\frac{N(d_{222} - d_{22-2})}{4h^2(d_{222} + d_{22-2})} \quad (4)$$

where N = 12 and h = 2 [28]. Furthermore, the phase content within the phase coexistence zone should be related to the relative intensities of the 200_c reflections. The volume fraction of the T phase (F_t) was approximately determined by:

$$F_t = SI_t/(SI_t + SI_o), \quad (5)$$

where SI_t and SI_o are the sums of peak intensities of 200_c reflections for T and O phases, respectively [29]. The volume fraction of the O phase (F_o) was then given by $F_o = 1 - F_t$.

3.2. Composition dependent lattice distortion and phase content

Fig. 2(a) and (b) show the synchrotron powder XRD patterns of 200_c and 222_c reflections for NKNS-xLT ceramics, respectively. It can be seen that O phase was dominant as x was below 0.03, as characterized by distinct $202_o/020_o$ and $22\text{-}2_o/222_o$ doublets. However, the phase structure changed into a typical T phase as x was beyond 0.04 due to an obvious $002_t/200_t$ doublet and a single 222_t reflection. As a result, the O-T PPB can be identified in the composition range of $0.03 \leq x \leq 0.04$. The calculated lattice distortion and phase content as a function of x are shown in Fig. 2(c) and (d), respectively. It is evident that δ_o was nearly constant (~0.64%) not only in the single O-phase zone but also within the O-T phase coexistence zone. However, δ_t was much larger than δ_o. It exhibited a very slight increase with x within PPB, but a drastic rise from ~0.93% at x = 0.04 to ~1.15% at x = 0.06. In the PPB region, both δ_o and δ_t showed little composition dependence, which is very similar to the variation of lattice distortion in PZT-based morphotropic compositions [23]. Unlike the lattice distortion, the phase content within PPB showed a quick change from F_t = 14% at x = 0.03 to F_t = 90% at x = 0.04 for T phases or vice versa for O phases, as shown in Fig. 2(d).

3.3. Composition dependent microstructure and domain structure

Fig. 3(a)–(c) show SEM images on the fractured surface for three selected compositions sintered at 1100 °C for 3 h. It can be seen that all samples were well densified (>95% theoretical densi-

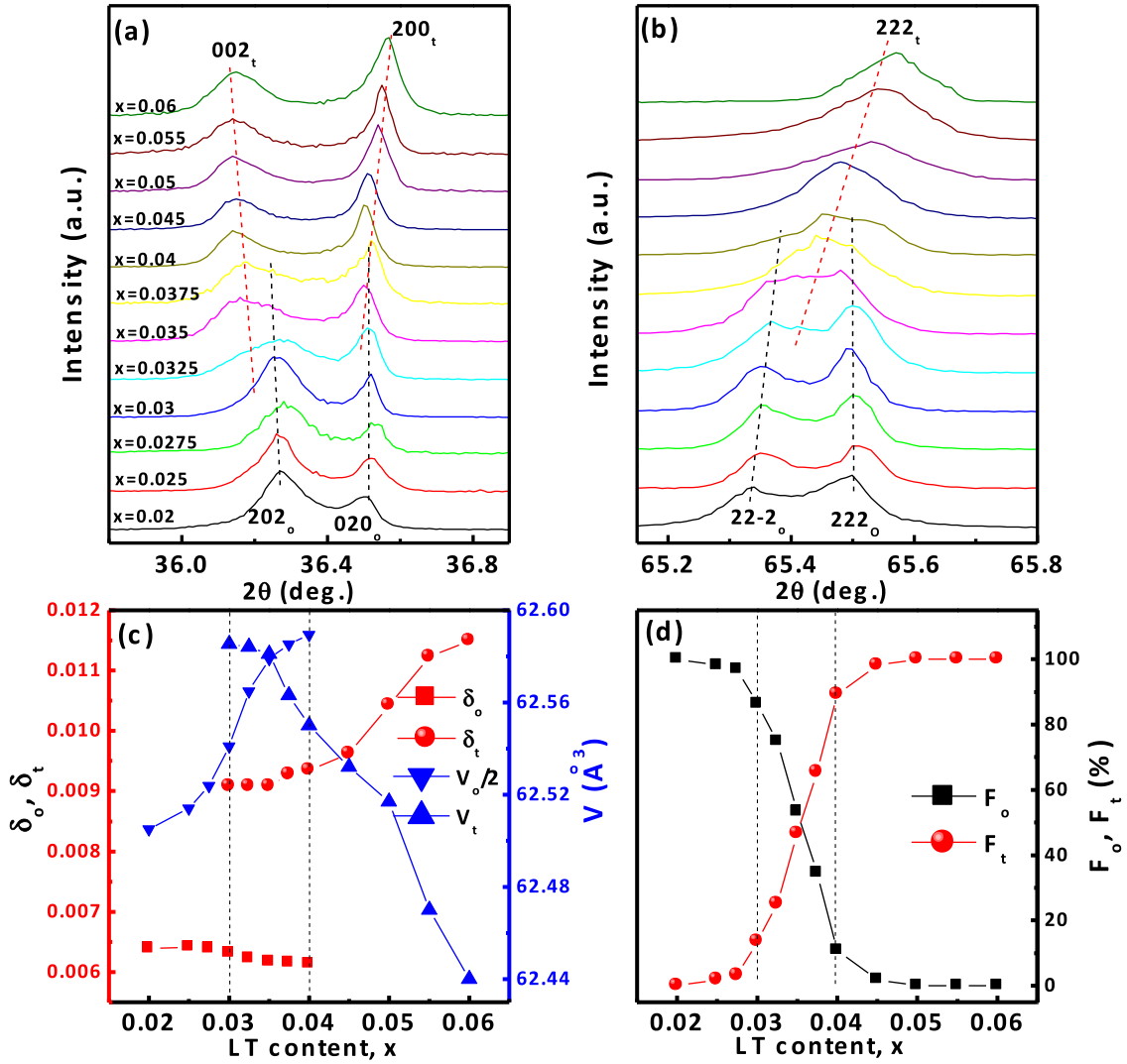

Fig. 2. The evolution of (a) 200_c and (b) 222_c reflections with varying x, and the corresponding (c) lattice distortion δ and unit cell volume V and (d) phase content F with changing x.

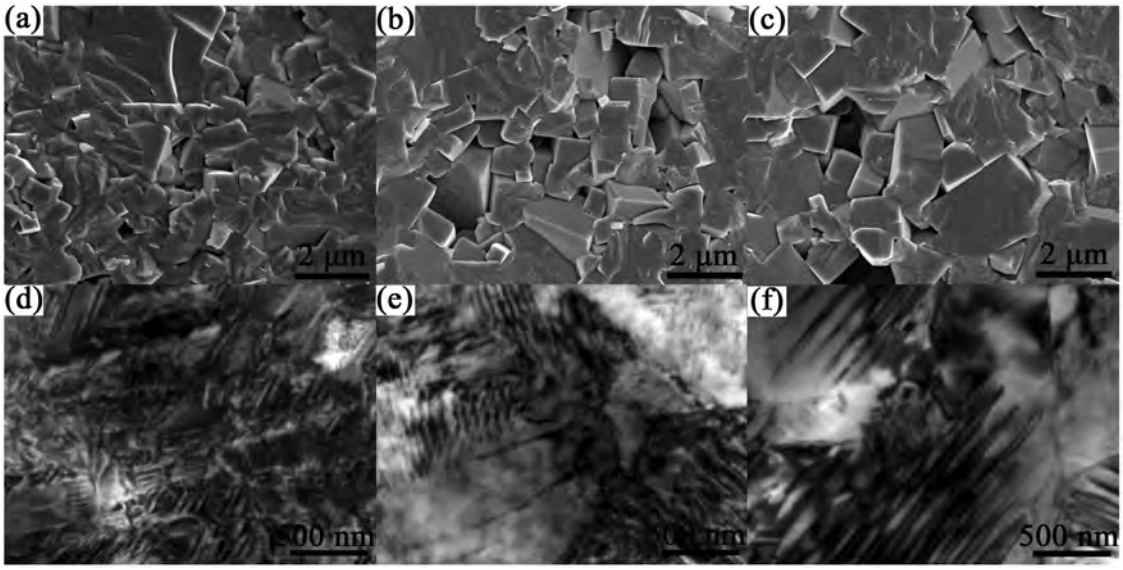

Fig. 3. SEM micrographs on the fractured surface of NKNS-xLT samples: (a) x = 0.02, (b) x = 0.0375 and (c) x = 0.045, and bright-field images for NKNS-xLT samples: (d) x = 0.02, (e) x = 0.0375 and (f) x = 0.045.

ties) with cubic grain morphology. The grain size slightly increased with increasing the LT content. In addition, the addition of LT was found to have an obvious effect on the domain structure probably because of the O-T phase structure change via an O-T PPB, as shown in Fig. 3(d)–(f). For a single O phase composition (x = 0.02), very irregular domains were observed. However, for the x = 0.0375 composition, typical T domains (top-left corner of Fig. 3(e)) with narrow lamellar patterns and O domains (bottom-right corner of Fig. 3(e)) with irregular patterns were observed, indicating the coexistence of O and T phases. With further increasing the LT content to x = 0.045, typical T domains with large parallel strips were observed.

3.4. Composition dependent domain switching behavior

As mentioned above, different domain switching behavior might be expected because of composition dependent phase structure and domain structure. The P-E loops of NKNS-xLT ceramics are shown in Fig. 4(a–c). The corresponding saturated polarization (P_{max}), remnant polarization (P_r) and coercive field (E_c) as a function of x are shown in Fig. 4(d). It can be seen that P_{max}, P_r and E_c within PPB showed less composition dependence than those in single-phase regions, which is in accordance with the variation of lattice distortion within PPB in Fig. 2(c). As the composition got closer to PPB, P-E loops became more rectangular, resulting in higher P_{max} and P_r values. This can be attributed to the easier reorientation of polarization vectors owing to the flattening of free energy profile within the phase coexistence zone. A rapid increase of δ_t in the single T-phase region with increasing x is responsible for a drastic increase of E_c from ~0.89 kV/mm at x = 0.04 to ~1.65 kV/mm at x = 0.06. Under a certain external electric field, the achieved P_{max} and P_r values could be small if the E_c of the sample is too large owing to the difficulty of domain switching. By comparison, in the single O-phase zone, E_c exhibited an unexpected increase from 0.66 kV/mm at x = 0.01 to 0.84 kV/mm at x = 0.03 because δ_o showed no obvious change. A possible explanation is that E_c should be correlated with not only the lattice distortion δ, but also the type of domains. The switching of non-180° domains was believed to be more difficult than that of 180° domains because the former involves mechanical stresses, which in turn limit their further switching and thus increase the E_c value. Therefore, a slight increase of E_c with increasing x in the O-phase zone might be attributed to an increase in the number of non-180° domains (or the density of non-180° domains). Moreover, the change of the domain type might be associated with the increase of the unit cell volume ($V_o/2$) of the O phase (see Fig. 2(c)), although the lattice distortion δ_o is almost constant. It is worthy of note that the E_c value showed little change with varying x within PPB (Fig. 4(d)). This is basically as a matter of fact that the lattice distortion δ values kept constant within the phase coexistence zone (Fig. 2(c)). Moreover, there might be another reason that the effect of mechanical stress from high-δ_t T-phase domain switching within O-T phase coexistence zone could be alleviated by low-δ_o O-phase domain switching. Interestingly, the change of E_c with x well explained the variation of the number of degenerate orientation (i.e., the variation of $\Delta P = P_{max} - P_r$) during electric cycling, which decreased from 9.45 μC/cm^2 at x = 0.01 to 5.08 μC/cm^2 approximately at x = 0.03. The ΔP value became nearly constant after a certain E_c, meaning that the number of reversible domain switching becomes stable as E_c is large enough.

3.5. Composition dependent macroscopic strains from S-E curves

Bipolar S-E curves of NKNS-xLT ceramics are shown in Fig. 5(a–c). All compositions exhibited a typical butterfly strain loop with an obvious negative strain (S_{neg}) as a result of irreversible non-180° domain switching [23]. By comparison, positive strain (S_{pos}) is mainly attributed to both the lattice strain (S_{piezo}) and reversible domain switching (S_{switch}). It can be seen from Fig. 5(a) and (d) that both S_{pos} and S_{neg} increased slightly in the O-phase zone from ~0.104% and ~0.052% at x = 0.01 to ~0.117% and ~0.067% at x = 0.03, respectively. By comparison, both of them decreased rapidly in the T-phase zone from ~0.141% and ~0.1% at x = 0.04 to ~0.096% and ~0.063% at x = 0.06, respectively, as shown in Fig. 5(c) and (d). In the PPB region, the change of S_{neg} and S_{pos} was complicated and could be divided into two regions, i.e., the O-rich side of PPB ($x \leq 0.035$) and T-rich side of PPB ($x > 0.035$). The variation of S_{neg} and S_{pos} at both O-rich side and T-rich side of PPB was very close to that in adjacent O-phase and T-phase compositions, respectively. The maximum S_{neg} and S_{pos} values appeared with PPB probably because of enhanced domain mobility. Different strain values in these compositions indicate that the strain contribution and its mechanism in each phase region should be different from each other.

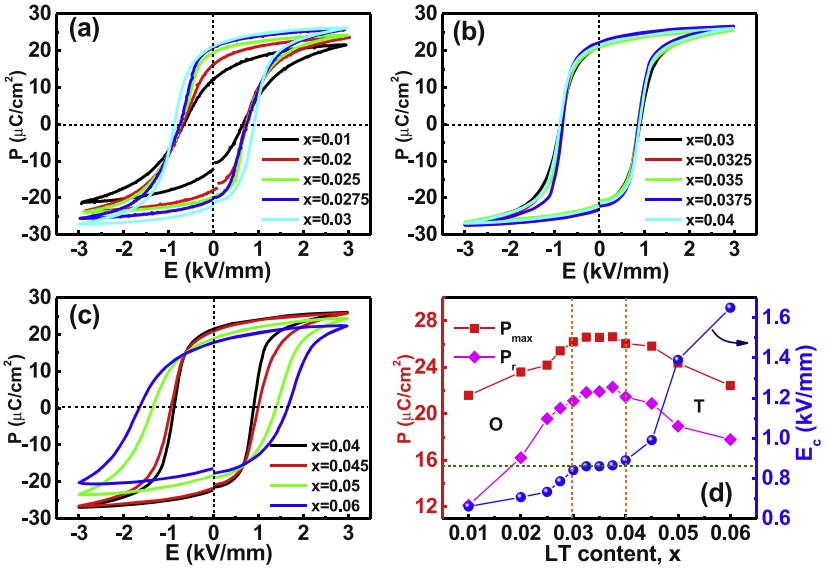

Fig. 4. P-E curves of NKNS-xLT ceramics with (a) x = 0.01–0.03 (O phase zone), (b) x = 0.03–0.04 (O-T PPB) and (c) x = 0.04–0.06 (T phase zone), and (d) the evolution of P_{max}, P_r and E_c values as a function of x.

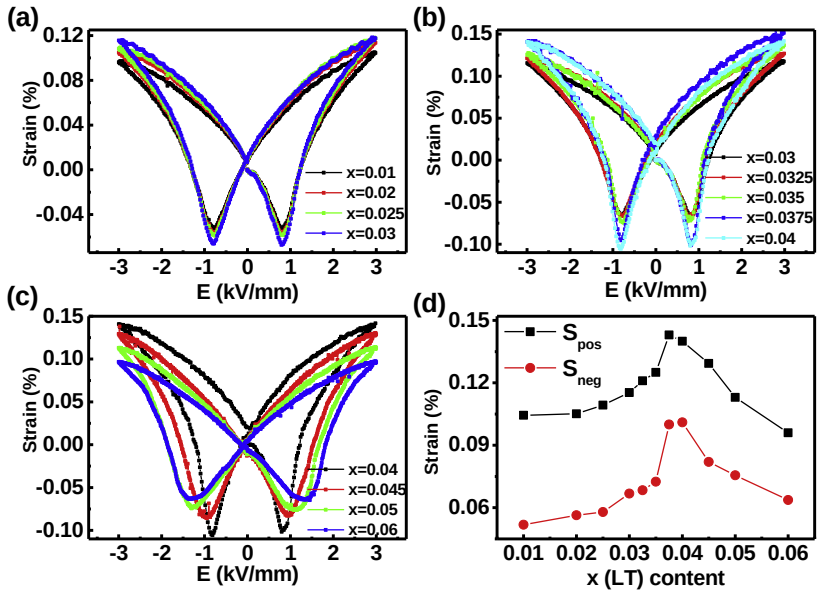

Fig. 5. Bipolar S-E curves of NKNS-xLT ceramics with (a) x = 0.01–0.03 (O phase zone), (b) x = 0.03–0.04 (O-T PPB) and (c) x = 0.04–0.06 (T phase zone), and (d) the evolution of S_{pos} and S_{neg} values as a function of x.

3.6. *Calculated strains from domain switching and piezoelectric effect*

To quantitatively characterize the strain contribution from non-180° domain switching, the 200_c reflections under different external field conditions are shown in Fig. 6 for a few selected NKNS-xLT samples. All compositions exhibited a considerable increase in the volume fraction of non-180° domains parallel to the applied electric field direction, as evidenced by the increase of the peak intensity ratios between the $202_o/020_o$ and $002_t/200_t$ reflections for the O and T phases, respectively. The volume fraction (f) of domains parallel to the poling direction for O and T phases can be expressed as follows:

$$f_o = I_{202_o} / \left(I_{202_o} + I_{020_O}\right) \quad (6)$$

$$f_t = I_{002_t} / \left(I_{200_t} + I_{002_t}\right) \quad (7)$$

For the random polycrystalline ferroelectric ceramics, f_o and f_t are expected to be ~66% and ~33% for O and T phases at the virgin state, respectively. The calculated results showed a good agreement for T-phase compositions, but a slight deviation for O-phase compositions (Fig. 7(a)), probably owing to the orientation effect from the ceramic disk. Because of the peak overlapping, f values of PPB compositions in Fig. 7(a) are neither f_o nor f_t, but should be their sums, thus depending on the phase content (F) in the range of 33–66% ($f = f_o \times F_o + f_t \times F_t$). Compared with virgin samples, f values under an electric field of 3 kV/mm increased up to 80–92% for O-rich compositions and to 45–60% for T-rich compositions. However, after removal of the electric field, only ~68–80% of O domains and ~40–48% of T domains were found to align towards the poling direction due to the depolarization process. Particularly, f values exhibited a much faster drop with increasing x in the O-phase zone than in the T-phase zone, although E_c increases with

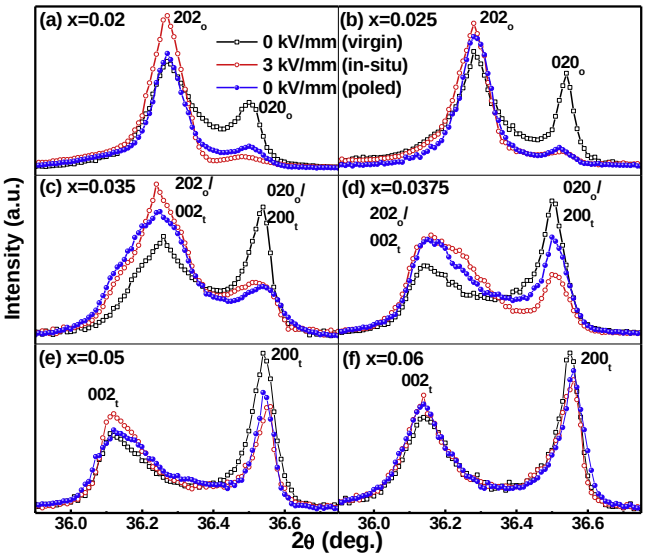

Fig. 6. Synchrotron XRD patterns of 200_c reflections in NKNS-xLT ceramics under various electric field conditions: (a) x = 0.02, (b) x = 0.025, (c) x = 0.035, (d) x = 0.0375, (e) x = 0.05 and (f) x = 0.06.

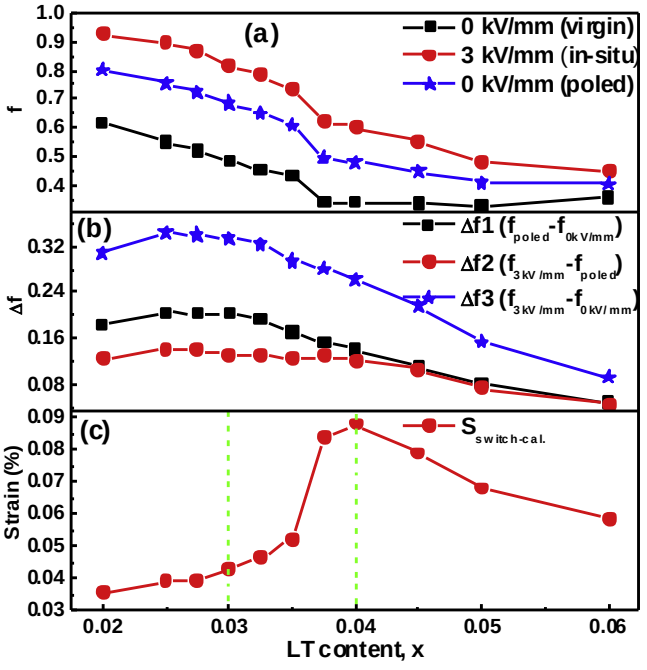

Fig. 7. (a) The volume fraction (f) of domains parallel to the poling direction and (b) degree of domain switching (Δf) under various electric field conditions, and (c) the calculated reversible domain switching strain ($S_{switch\text{-}cal.}$) as a function of x.

x more rapidly in the T phase zone than in the O phase zone. This is probably because the type of domains of O phases can be more influenced by the change of the unit cell volume.

Fig. 7(b) shows the degree of domain switching under various field conditions, as denoted by Δf_1 ($=f_{poled} - f_{0\,kV/mm}$), Δf_2 ($=f_{3\,kV/mm} - f_{poled}$) and Δf_3 ($=f_{3\,kV/mm} - f_{0\,kV/mm}$), respectively. Here, Δf_1 and Δf_2 represent the degrees of irreversible and reversible non-180° domain switching, respectively, and Δf_3 is the degree of total non-180° domain switching. On the one hand, all of them were higher in O-rich phase zone than in T-rich phase zone, illustrating that domain switching of the O phase is generally easier than that of the T phase. On the other hand, Δf values were relatively independent of the compositional change in the O-phase zone compared with the T-phase zone. The magnitude of Δf illustrates the degree of domain switching under the external electric fields, which should be suppressed with increasing the lattice distortion δ. This should explain why Δf obviously decreased with increasing x in the T-phase zone.

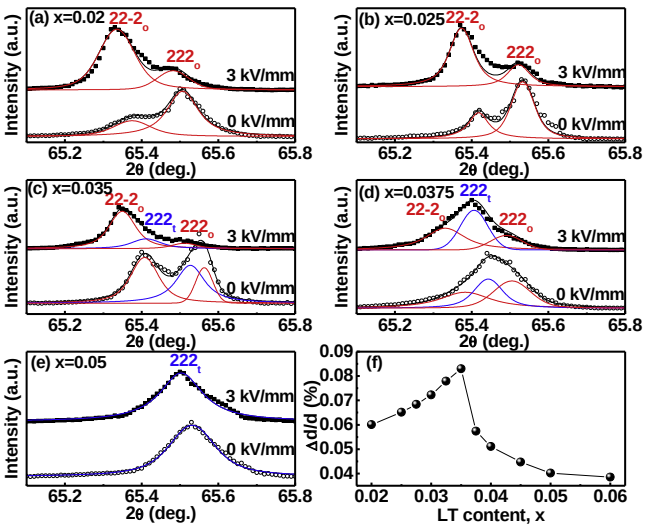

Fig. 8. (a–e) In-situ synchrotron XRD patterns of 222_c reflections of NKNS-xLT samples as indicated, which were fitted by using a pseudo-Voigt function and (f) the lattice spacing change (Δd/d) from 222_c reflections as a function of x.

Fig. 7(c) shows the calculated strain values from reversible domain switching ($S_{switch-cal.}$) as a function of x. $S_{switch\text{-}cal.}$ ($\Delta f_2 \times S_{neg}/\Delta f_1$) in the single phase zone is calculated based on the assumption that the change of strain is proportional to the poling texture change [23]. In the PPB region, $S_{switch\text{-}cal.}$ can also be obtained by regarding the O phase and the T phase as a whole, in which the phase content and lattice distortion of each composition keep constant during poling. It is obvious that $S_{switch-cal.}$ values with a level of ~0.06–0.087% were observed in T-rich compositions. These values are much larger than those of O-rich compositions. However, the $S_{switch\text{-}cal.}$ value in the single O phase region exhibited much less composition dependence than that in the T-phase region, which should be mainly due to the different dependence of δ on composition in these two phase regions. In the PPB region, $S_{switch\text{-}cal.}$ rapidly increased with increasing x from 0.03 to 0.04. The highest $S_{switch-cal.}$ of ~0.088% appeared in the composition of x = 0.04, which is just located at the crossover between the PPB region and the single T-phase region. The basic reason for this should be based on the fact that the hindrance to domain switching within PPB was minimized owing to the phase coexistence.

Fig. 8(a–e) show in-situ synchrotron XRD on 222_c reflections of a few selected NKNS-xLT compositions under electric fields of 0 and 3 kV/mm. All compositions exhibited a considerable change of peak positions, as can be seen from the shift of the $22\text{-}2_o$ reflection for the O phase and the 222_t reflection for the T phase. By comparison, the lattice strain observed from other reflections was very small for both O-phase and T-phase compositions. Particularly, it can be seen from Fig. 6 that the lattice strain from 200_c reflections was negligible because the peak position of the 200_c reflections seemed to be independent of the field condition. The peak position (2θ) of $22\text{-}2_o$ and 222_t reflections, which was obtained by peak fitting with a pseudo-Voigt function, was then used to calculate the lattice strain of O and T phases, respectively, according to the following equations:

$$\varepsilon_{22-2} = \frac{\Delta d}{d} \times 100\% = \frac{d'_{22-2} - d_{22-2}}{d_{22-2}} \times 100\% \quad (8)$$

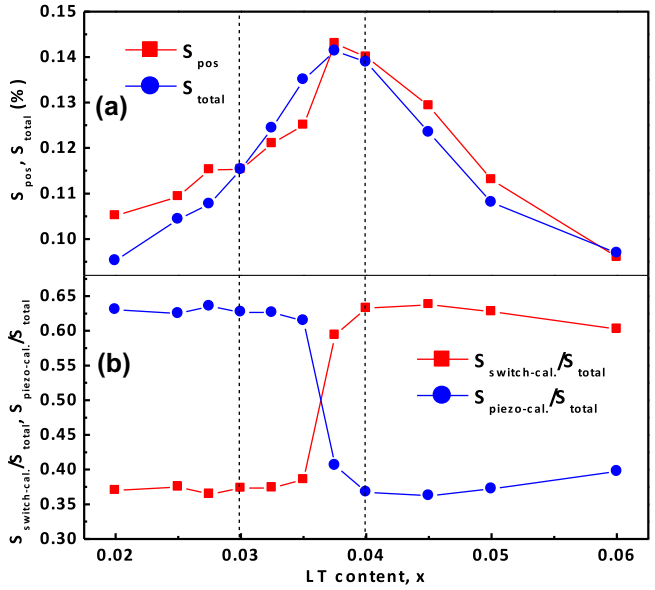

Fig. 9. (a) The S_{pos} and S_{total} with changing x, and (b) the variation in the fraction of intrinsic contribution ($S_{piezo-cal.}/S_{total}$) and extrinsic contribution ($S_{switch-cal.}/S_{total}$) in relative to the unipolar strain as a function of x.

$$\varepsilon_{222} = \frac{\Delta d}{d} \times 100\% = \frac{d'_{222} - d_{222}}{d_{222}} \times 100\% \quad (9)$$

where, d'_{22-2}, d_{22-2}, d'_{222}, and d_{222} represent 22-2_o lattice spacings under 3 kV/mm and 0 kV/mm for O-phase compositions and 222_t lattice spacings under 3 kV/mm and 0 kV/mm for T-phase compositions, respectively. In the PPB region, the lattice strain should be the sum of the lattice strain of each phase weighted with the corresponding phase fraction because the peak shift can be seen in both 22-2_o and 222_t reflections. It is generally believed that the lattice strain along nonpolar (or polar) directions due to the polarization rotation (or polar extension) can give an indication of the macroscopic piezoelectric strain in ferroelectric ceramics. In the present study, the lattice strain along nonpolar 222_c direction can be mirrored closely to the macroscopic longitudinal piezoelectric strain in NKN-based ceramics. However, this method may be more suitable for the materials with a strong polarization rotation. As shown in Fig. 8(f), the calculated lattice strain $S_{piezo-cal.}$ ($\Delta d/d$) first increased slightly until x = 0.035, and then decreased rapidly with further increasing x. As a result, $S_{piezo-cal.}$ at the O-rich phase zone was obviously larger than at the T-rich phase zone.

By assuming that there is no contribution from the field induced phase transition, the calculated total strain (S_{total}), which is the sum of both $S_{piezo-cal.}$ and $S_{switch-cal.}$ ($S_{total} = S_{piezo-cal.} + S_{switch-cal.}$), should approximate to the macroscopic unipolar strain (i.e., S_{pos}). Fig. 9(a) shows a comparison of the measured S_{pos} from S-E curves and the calculated S_{total} from diffraction data. It can be seen that the calculated values kept a good agreement with the measured ones, indicating that the theoretical calculation via a specific reflection in present study is a valid estimation of the strain contribution of NKN-based compositions. Fig. 9(b) shows the fraction of the intrinsic contribution and the extrinsic contribution. It is worthy of note that reversible non-180° domain switching in T-rich compositions (x > 0.035) took up to ~60–63% of the total unipolar strain. On the contrary, the piezoelectric lattice strain accounted for ~61–63% of the unipolar strain for O-rich compositions (x < 0.035). The result indicates that strain contributions were dominated by a large extrinsic contribution for T-rich compositions, compared with O-rich compositions with a dominant intrinsic contribution. Some other studies also found that extrinsic contribution from domain switching in NKN-based systems became dominant as compositions crossed the phase boundary into the T-phase zone [30,31].

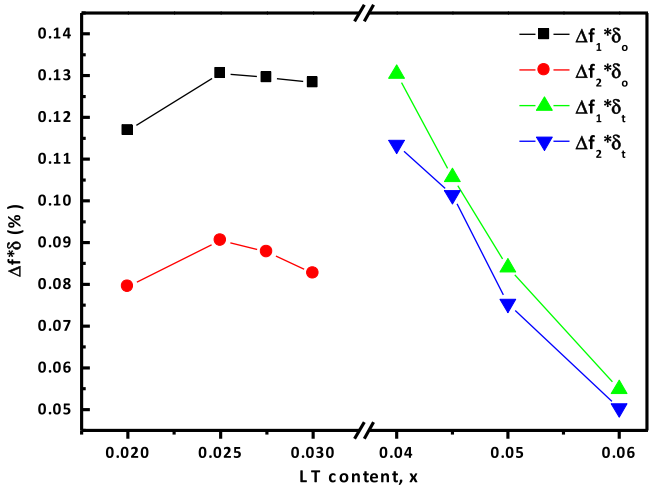

Fig. 10. The composition dependent $\Delta f \times \delta$ values under different electric field conditions for O-phase and T-phase compositions.

4. Discussion

The strain magnitude from non-180° domain switching generally depends on the degree of lattice distortion. However, the variation of S_{neg} and $S_{switch-cal.}$ with varying x in this study (see Fig. 5(d) and Fig. 7(c)) was found to be inconsistent with the change of δ. It became more pronounced for single T-phase compositions in which an obvious decrease of extrinsic strains accompanied a rapid increase of δ_t. This phenomenon can be ascribed to the fact that non-180° domain switching necessarily involves mechanical stresses, which instead constrain the domain switching. As a result, a reasonable domain switching strain has to be estimated by balancing the effect of δ and Δf. From Figs. Fig. 77(b) and Fig. 22(c), one can see that the degree of domain switching decreased significantly in the range of $0.04 \leq x \leq 0.06$ (from ~14% to ~4.7% for Δf_1 and from ~12% to ~4.3% for Δf_2) together with a moderate increase in δ_t from ~0.93% to ~1.15%. By comparison, only a slight change of Δf and a nearly composition-independent δ_o could be observed in the single O-phase region. Fig. 10 shows $\Delta f \times \delta$ values as a function of x, which generally approximate to S_{neg} ($\Delta f_1 \times \delta_o$ (δ_t)) and $S_{switch-cal.}$ ($\Delta f_2 \times \delta_o$ (δ_t)) values. It can be seen that the estimated S_{neg} was much higher than the estimated $S_{switch-cal.}$ in the single O-phase zone. Smaller lattice distortion (Fig. 2(c)) and higher poling texture (Fig. 7(b)) for O phases tend to drive the texture of a poled state close to the saturation limit [32], meaning the amount of reversible domain switching was largely limited in O-phase compositions (Fig. 7(c)). For the same reason, the amount of reversible domain switching would obviously increase with increasing δ, such that reversible and irreversible domain switching strains are comparable within PPB and even in single T-phase zone. It has been proposed in previous studies that the polarization rotation represented by the lattice strains along nonpolar directions in polycrystalline ceramics can be considered as a result of coupling between the elastic strain and the irreversible non-180° domain switching [21,33]. This might also explain why a relatively large intrinsic strain ($S_{piezo-cal.}$) was observed in the O-phase region in current study due to its high Δf1. For PPB compositions, both domain switching strains and piezoelectric lattice strains should depend on the phase content in addition to the lattice distortion and degree of poling texture.

Furthermore, it is worthy of note that both $\Delta f_1 \times \delta_t$ and $\Delta f_2 \times \delta_t$ values in single T-phase zone kept a good agreement with the

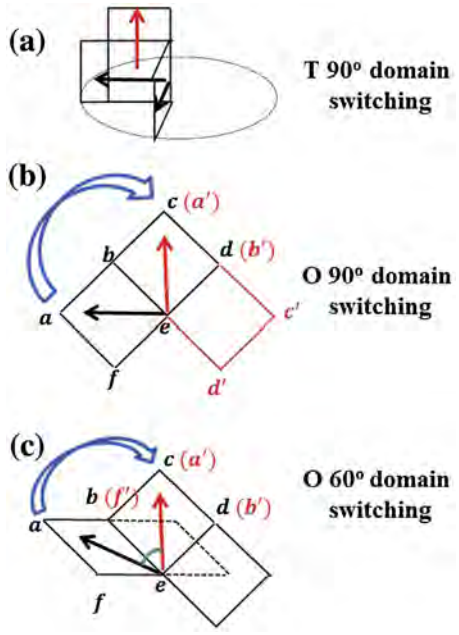

Fig. 11. Schematic illustrations of (a) T 90° domain switching, (b) O 90° domain switching and (c) O 60° domain switching.

measured S_{neg} (Fig. 5(d)) and $S_{switch\text{-}cal.}$ values (Fig. 7(c)), respectively. However, $\Delta f_1 \times \delta_o$ and $\Delta f_2 \times \delta_o$ in single O-phase zone were twice more than S_{neg} and $S_{switch\text{-}cal.}$, respectively. The result means that compared with T-phase compositions, there should be an additional factor to affect the domain switching for O-phase compositions, i.e., the type of domains being switched. There are two types of domains in T phase, i.e., 90° domains and 180° domains, while O phases are composed of 90°, 60°, 120° and 180° domains. Only non-180° domains are discussed here because 180° domains do not contribute to the strain. Fig. 11 shows the sketches of typical T domain switching and O domain switching. It can be seen from Fig. 11(a) and (b) that the strain from T 90° domain switching and O 90° domain switching should equal to δ_t and δ_o, respectively, when domains are fully reoriented along the external field direction. By comparison, O 60° domain switching (the effect of 120° and 60° domain switching is equivalent) is more complicated, and shows a less strain contribution than 90° domain switching, as shown in Fig. 11(c). As we know, among $\{110\}_c$ planes, $(101)_c$ and $(-10-1)_c$ planes are parallel and antiparallel to the $(101)_c$, both $(10-1)_c$ and $(-101)_c$ planes are perpendicular to the $(101)_c$ plane, and the angles between the other eight planes and $(101)_c$ plane are 60°/120°. This hints the O phase should be dominated by 60°/120° domains rather than 90° domains. Therefore, the calculation of $\Delta f_1 \times \delta_o$ and $\Delta f_2 \times \delta_o$ in single O-phase zone would overestimate the actual S_{neg} and $S_{switch-cal.}$ owing to a lower strain contribution of 60°/120° domains than 90° domains. That is to say, the theoretical calculation of S_{neg} and S_{switch} using the multiplication of Δf and δ should better fit T-rich compositions.

5. Conclusions

Domain switching behavior and underlying strain mechanisms of typical NKNS-xLT lead-free ferroelectric ceramics were investigated by using high-energy synchrotron XRD in combination with macroscopic strain measurements. Although domain switching is more difficult in single T phase than in single O phase, yet lower strain contribution and lattice distortion and thus higher poling textures for O phases resulted in lower extrinsic strain contributions from non-180° domain switching but higher piezoelectric lattice strains. In the PPB region, strains from irreversible and reversible domain switching in both O-rich side and T-rich side of PPB were higher than those of adjacent O phase and T phase compositions, respectively, owing to enhanced domain wall mobility. In addition, strains from irreversible domain switching were found to be much higher than those from reversible domain switching possibly for O-phase compositions but they are comparable for PPB compositions and T-phase compositions. An overestimation of domain switching strains by $\Delta f \times \delta$ suggests that extrinsic strain contributions should depend on not only the lattice distortion δ and the poling texture Δf, but also domain types and phase contents (for PPB compositions).

Acknowledgements

This work was supported by the National Natural Science Foundation of China (Grants No. 51472069, U1432113, 51402079, 51332002) and the Anhui Provincial Natural Science Foundation (1508085JGD04).

References

[1] C.S. Lynch, The effect of uniaxial stress on the electro-mechanical response of 8/65/35 PLZT, Acta Mater. 44 (1996) 4137–4148.
[2] K. Uchino, Materials issues in design and performance of piezoelectric actuators: an overview, Acta Mater. 46 (1998) 3745–3753.
[3] K. Bhattacharya, G. Ravichandran, Ferroelectric perovskites for electromechanical actuation, Acta Mater. 51 (2003) 5941–5960.
[4] Y. Saito, H. Takao, T. Tani, T. Nonoyama, K. Takatori, T. Homma, T. Nagaya, M. Nakamura, Lead-free piezoceramics, Nature 432 (2004) 84–87.
[5] E. Hollenstein, M. Davis, D. Damjanovic, N. Setter, Piezoelectric properties of Li- and Ta-modified $(K_{0.5}Na_{0.5})NbO_3$ ceramics, Appl. Phys. Lett. 87 (2005) 182905.
[6] E.K. Akdogan, K. Kerman, M. Abazari, A. Safari, Origin of high piezoelectric activity in ferroelectric $(K_{0.44}Na_{0.52}Li_{0.04})(Nb_{0.84}Ta_{0.1}Sb_{0.04})O_3$ ceramics, Appl. Phys. Lett. 92 (2008) 112908.
[7] R.Z. Zuo, J. Fu, D.Y. Lv, Phase transformation and tunable piezoelectric properties of lead-free $(Na_{0.52}K_{0.48-x}Li_x)(Nb_{1-x-y}Sb_yTa_x)O_3$ system, J. Am. Ceram. Soc. 92 (2009) 283–285.
[8] K. Wang, J.F. Li, J.J. Zhou, High normalized strain obtained in Li-modified $(K,Na)NbO_3$ lead-free piezoceramics, Appl. Phys. Exp. 4 (2011) 061501.
[9] R.Z. Zuo, J. Fu, G.Z. Yin, X.L. Li, J.Z. Jiang, Electric field induced phase instability in typical $(Na,K)(Nb,Sb)O_3$-$LiTaO_3$ ceramics near orthorhombic and tetragonal phase boundary, Appl. Phys. Lett. 101 (2012) 092906.
[10] K. Yan, X.B. Ren, Multi-phase transition behavior and large electrostrain in lead-free $(K,Na,Li)NbO_3$ ceramics, J. Phys. D: Appl. Phys. 47 (2014) 015309.
[11] J. Fu, R.Z. Zuo, S.C. Wu, J.Z. Jiang, L. Li, T.Y. Yang, X.H. Wang, L.T. Li, Electric field induced intermediate phase and polarization rotation path in alkaline niobate based piezoceramics close to the rhombohedral and tetragonal phase boundary, Appl. Phys. Lett. 100 (2012) 122902.
[12] T. Zheng, J.G. Wu, X.J. Cheng, X.P. Wang, B.Y. Zhang, D.Q. Xiao, J.G. Zhu, X.J. Wang, X.J. Lou, High strain in $(K_{0.40}Na_{0.60})(Nb_{0.955}Sb_{0.045})O_3$-$Bi_{0.50}Na_{0.50}ZrO_3$ lead-free ceramics with large piezoelectricity, J. Mater. Chem. C 2 (2014) 8796.
[13] S.Y. Choi, S.J. Jeong, D.S. Lee, M.S. Kim, J.S. Lee, J.H. Cho, B.I. Kim, Y. Ikuhara, Gigantic electrostrain in duplex structured alkaline niobates, Chem. Mater. 24 (2012) 3363–3369.
[14] F.Z. Yao, J. Glaum, K. Wang, W. Jo, J. Rodel, J.F. Li, Fatigue-free unipolar strain behavior in $CaZrO_3$ and MnO_2 co-modified $(K,Na)NbO_3$-based lead-free piezoceramics, Appl. Phys. Lett. 103 (2013) 192907.
[15] K. Wang, F.Z. Yao, W. Jo, D. Gobeljic, V.V. Shvartsman, D.C. Lupascu, J.F. Li, J. Rodel, Temperature-insensitive $(K,Na)NbO_3$-based lead-free piezoactuator ceramics, Adv. Funct. Mater. 23 (2013) 4079–4086.
[16] K. Uchino, Ferroelectric Devices, Marcel Dekker, New York, 2009.
[17] A. Pramanick, D. Damjanovic, J.E. Daniels, J.C. Nino, J.L. Jones, Origins of electro-mechanical coupling in polycrystalline ferroelectrics during subcoercive electrical loading, J. Am. Ceram. Soc. 94 (2011) 293–309.
[18] J. Wang, W. Shu, T. Shimada, T. Kitamura, T.-Y. Zhang, Role of grain orientation distribution in the ferroelectric and ferroelastic domain switching of ferroelectric polycrystals, Acta Mater. 61 (2013) 6037–6049.
[19] N.H. Khansur, H. Kawashima, S. Wada, J.M. Hudspeth, J. Daniel, Enhanced extrinsic domain switching strain in core-shell structured $BaTiO_3$-$KNbO_3$ ceramics, Acta Mater. 98 (2015) 182–189.
[20] J.T. Reszat, A.E. Glazounov, M.J. Hoffmann, Analysis of intrinsic lattice deformation in PZT-ceramics of different compositions, J. Eur. Ceram. Soc. 21 (2001) 1349–1352.
[21] D.A. Hall, A. Steuwer, B. Cherdhirunkorn, T. Mori, P.J. Withers, A high energy synchrotron x-ray study of crystallographic texture and lattice strain in soft lead zirconate titanate ceramics, J. Appl. Phys. 96 (2004) 4245–4252.

[22] J.L. Jones, E.B. Slamovich, K.J. Bowman, Domain texture distribution in tetragonal lead zirconate titanate by x-ray and neutron diffraction, J. Appl. Phys. 97 (2005) 034113.
[23] H. Kungl, R. Theissmann, M. Knapp, C. Baehtz, H. Fuess, S. Wagner, T. Fett, M.J. Hoffmann, Estimation of strain from piezoelectric effect and domain switching in morphotropic PZT by combined analysis of macroscopic strain measurements and synchrotron X-ray data, Acta Mater. 55 (2007) 1849–1861.
[24] M. Hinterstein, M. Hoelzel, J. Rouquette, J. Haines, J. Glaum, H. Kungl, M. Hoffman, Interplay of strain mechanisms in morphotropic piezoceramics, Acta Mater. 94 (2015) 319–327.
[25] L.L. Fan, J. Chen, Y. Ren, Z. Pan, L.X. Zhang, X.R. Xing, Unique piezoelectric properties of the monoclinic phase in Pb(Zr, Ti)O_3 ceramics: large lattice strain and negligible domain switching, Phys. Rev. Lett. 116 (2016) 027601.
[26] D.K. Khatua, K.V. Lalitha, C.M. Fancher, J.L. Jones, R. Ranjan, Anomalous reduction in domain wall displacement at the morphotropic phase boundary of the piezoelectric alloy system $PbTiO_3$-$BiScO_3$, Phys. Rev. B 93 (2016) 104103.
[27] J. Tellier, B. Malic, B. Dkhil, D. Jenko, J. Cilensek, M. Kosec, Crystal structure and phase transitions of sodium potassium niobate perovskites, Solid State Sci. 11 (2009) 320–324.
[28] V.J. Tennery, High-temperature phase transitions in $NaNbO_3$, J. Am. Ceram. Soc. 48 (1965) 537–539.
[29] C.W. Ahn, C.S. Park, D. Viehland, S. Nahm, D.H. Kang, K.S. Bae, S. Priya, Correlation between phase transitions and piezoelectric properties in lead-free (K,Na,Li)NbO_3-$BaTiO_3$ ceramics, Jpn, J. Appl. Phys. 47 (2008) 8880–8883.
[30] T. Iamsasri, G. Tutuncu, C. Uthaisar, S. Pojprapai, J.L. Jones, Analysis methods for characterizating ferroelectric/ferroeelastic domain reorientation in orthorhombic perovskite materails and application to Li-doped $Na_{0.5}K_{0.5}NbO_3$, J. Mater. Sci. 48 (2013) 6905–6910.
[31] D.A. Ochoa, G. Esteves, T. Iamsasri, F. Rubio-Marcos, J.F. Fernandez, J.E. Garcia, J.L. Jones, Extensive domain wall contribution to strain in a (K,Na)NbO_3-based lead-free piezoceramics quantified from high energy X-ray diffraction, J. Eur. Ceram. Soc. 36 (2016) 2489–2494.
[32] H. Kungl, M.J. Hoffmann, Temperature dependence of poling strain and strain under high electric fields in LaSr-doped morphotropic PZT and its relation to changes in structural characteristics, Acta Mater. 55 (2007) 5780–5791.
[33] D.A. Hall, A. Steuwer, B. Cherdhirunkorn, T. Mori, P.J. Withers, Analysis of elastic strain and crystallographic texture in poled rhombohedral PZT ceramics, Acta Mater. 54 (2006) 3075–3083.